ACS APPLIED MATERIALS & INTERFACES

www.acsami.org

Research Article

A First Molecular Dynamics Study for Modeling the Microstructure and Mechanical Behavior of Si Nanopillars during Lithiation

Fei Shuang and Katerina E. Aifantis*

Cite This: *ACS Appl. Mater. Interfaces* 2021, 13, 21310–21319

Read Online

ACCESS | Metrics & More | Article Recommendations | Supporting Information

ABSTRACT: This is the first study that employs large-scale atomistic simulations to examine the stress generation and deformation mechanisms of various Si nanopillars (SiNPs) during Li-ion insertion. First, a new robust and effective minimization approach is proposed to relax a lithiated amorphous SiNP (a-SiNP), which outperforms the known methods. Using this new method, our simulations are able to successfully capture the experimental morphological changes and volume expansions that SiNPs, hollow a-SiNPs, and solid crystalline SiNPs (c-SiNPs) experience upon maximum lithiation. These simulations enable us to selectively track the displacement of Si atoms and their atomic shear strain in the $Li_{3.75}Si$ alloy region, allowing us to observe the plastic flow and illustrate the atomistic mechanism of lithiation-induced deformation for various SiNPs for the first time. Based on the simulation results, a simple fracture mechanistic model is used to determine the fracture resistance of SiNPs, showing that the hollow a-SiNP is the optimal form of Si as an anode because it has the highest fracture resistance. The crack propagation simulation suggests that the preexisting dislocations in pristine c-Si can contribute toward the fracture of c-SiNPs during lithiation. These findings can guide the design of new Si-based anode geometries for the next-generation Li-ion batteries.

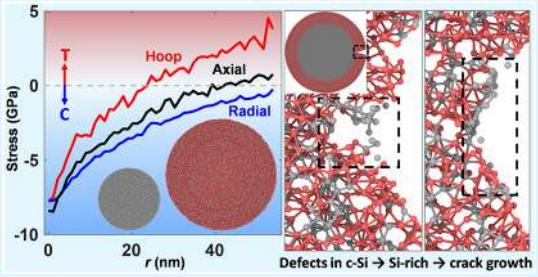

KEYWORDS: *Si anodes, Li-ion batteries, fracture, structural relaxation, atomistic simulation*

1. INTRODUCTION

Li-ion batteries (LIBs) have been widely used in electric vehicles, portable electronic devices, and grid-level energy storage owing to their high energy density, high power capability, and long lifetime.[1] One of the most promising anode materials is Si because of its high theoretical capacity of 4200 mA h/g, which is approximately 11 times that of commercially used graphitic anodes (372 mA h/g).[2] The alloying mechanism by which one Si mole hosts up to 4.4 Li moles is the key to this high capacity; however, it induces an enormous volume expansion (~400%), leading to the fracture and pulverization of Si and a fast capacity fade during the first several charge−discharge cycles.[3,4] Scanning electron microscopy (SEM) studies have revealed that the anomalous shape changes and fracture behavior of crystalline Si nanopillars (c-SiNPs) result from anisotropic lithiation,[5] while in situ transmission electron microscopy studies showed that the lithiation of Si occurs by the movement of an atomically sharp interface (~1.0 nm thick) which separates the lithiated shell (amorphous Li_xSi) and the crystalline Si core.[6]

Significant efforts are dedicated in developing mechanically stable Si anodes. Most of these studies are experimental and produce new material chemistries and geometries for Si-based anodes.[7−9] However, it was soon recognized that theoretical studies are also necessary to understand and, hence, minimize fracture in Si. Initial mechanics studies employed linear elasticity[10] and linear fracture mechanics[11,12] for capturing the stresses developed in anode particles experiencing volume expansions over 300%. Since then, computational simulations have been widely used to model the stress generation, anisotropic volume expansions, and fracture of Si by using chemo-mechanical models implemented in the finite element method,[13,14] phased field modeling,[15] and atomistic simulation.[16] Chemomechanical finite element modeling showed that hollow amorohousSiNPs (a-SiNPs) have a lower stress-induced barrier of lithiation than solid a-SiNPs.[17] By considering two-step lithiation in a-Si, it was also shown that a-Si particles have a better fracture resistance and experience a lower mechanical energy barrier than c-Si.[18] A robust electrochemical-mechanical couple numerical procedure was proposed[19] and was used to successfully capture the anisotropic expansion and stress generation in c-Si nanotubes.[20] A multiphysics phase-field model was used to capture crack patterns in Si thin films[21] and was recently applied in analyzing stress and damage in anodes of sodium-ion

Received: February 13, 2021
Accepted: April 9, 2021
Published: April 29, 2021

https://doi.org/10.1021/acsami.1c02977
ACS Appl. Mater. Interfaces 2021, 13, 21310−21319

batteries.[22] Without the need for a priori constitutive parameters as input, atomistic simulations have been successfully used to understand the fracture behavior of Li_xSi alloys,[23−25] the stress effect on lithiation,[26,27] and the structural changes of Si anodes during delithiation.[28,29] In particular, it was found that there exists a transition from cavitation to shear banding as the Li concentration increases,[24] which is consistent with the high damage tolerance of electrochemically lithiated Si as revealed in in-situ experiments.[30] Atomistic simulations based on the reactive force field (ReaxFF) also showed that external stresses significantly influence the lithiation rate,[27] which can explain the bending-induced symmetry breaking in germanium nanowires during lithiation in experiments.[31] A "natural" delithiation algorithm was designed to investigate the influence of the delithiation rate on the mechanical durability of Si anodes, showing that fast delithiation resulted in a higher irreversible capacity loss compared to slow delithiation.[28]

Although insightful, the aforementioned MD works could not implement physical lithiation into large-scale atomistic models. Consequently, they failed to capture the microstructural changes and stress generated in a-Si and c-Si during lithiation. Two recent atomistic simulations obtained the isotropic and anisotropic volume expansions of SiNPs with a diameter of 10.0 nm,[32,33] but the generated stresses were different from previous theoretical predictions.[17,18,34] Moreover, the atomistic mechanisms giving rise to plastic flow of Li_xSi alloys and lithiation-induced fracture have not been studied.

Particularly, even though plasticity is challenging to observe experimentally[35] since fracture dominates the mechanical behavior of Si upon lithiation, recent theoretical studies have shown that mechanical models that account for plasticity can better explain the observed fracture behavior of Si.[36,37] Therefore, in this work, large-scale atomistic simulations are employed to study the mechanical behavior (plasticity initiation/fracture) and morphology of various SiNPs, including solid a-SiNPs and c-SiNPs, as well as hollow a-SiNPs (with a maximum diameter of 60.0 nm) during lithiation. First, we test existing minimization methods such as the conjugate gradient (CG) method and the fast inertial relaxation engine (FIRE) method and find that they fail to generate reasonable lithiation-induced stresses and shape changes in an a-SiNP (Figure S2). To handle this special structural relaxation task, we propose a new robust and effective structural relaxation approach to simulate the lithiation process. The obtained shape changes and stress distributions of all SiNPs are compared with previous experiments and theoretical predictions. In addition to observing plastic deformation for the first time, we also studied fracture by inducing a crack and monitoring its propagation. Therefore, our work presents new simulations that not only complement existing experimental studies but further reveal the mechanical effects of lithiation, which are difficult to monitor otherwise.

2. METHODS

2.1. Simulation Setup and Empirical Potential. We consider the lithiation of solid amorphous Si nanopillars (a-SiNP), solid crystalline Si nanopillars (c-SiNP), and hollow a-SiNPs as illustrated in Figure 1. For a-SiNPs, three diameters (D) are considered in order to study the size effect: 10.0, 20.0, and 30.0 nm. The largest a-SiNP contains 299,200 Si atoms. The initial radius of a-SiNP before lithiation is R_0. It becomes r_0 after lithiation, during which a material

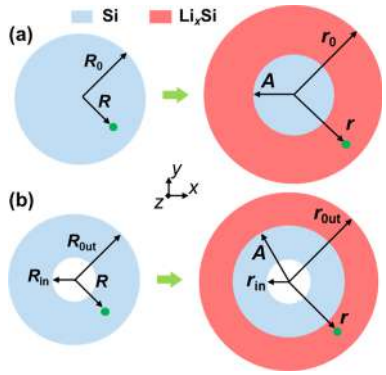

Figure 1. SiNP configurations. (a) Solid and (b) hollow SiNPs before and after lithiation.

point at a radius R moves to a new location at a radius r (Figure 1a), where A is the location of the lithiation front. Three c-SiNPs with the same diameter of 30.0 nm, but different axial directions are considered: ⟨110⟩ c-SiNP, ⟨100⟩ c-SiNP, and ⟨111⟩ c-SiNP. The hollow a-SiNPs are obtained by removing the Si atoms within the inner cylinder of radius R_{in} and expanding the outer radius to R_{out}.

The geometry of the hollow a-SiNPs satisfy $R_{out}^2 - R_{in}^2 = R_0^2$ (R_0 = 30.0 nm) such that hollow a-SiNPs and solid a-SiNPs contain the same number of Si atoms (keeping the volume constant for different a-SiNPs), where R_{out} and R_{in} represent the initial outer radius and inner radius, respectively. Hollow a-SiNPs are deformed with an inner radius of r_{in} and an outer radius of r_{out} after lithiation (Figure 1b). Four hollow cases with R_{in} = 5.0, 10.0, 20.0, and 30.0 nm are examined. The wall thickness of hollow SiNPs decreases with increasing R_{in}.

For all SiNPs, free boundary conditions are imposed in the x- and y-directions, and periodic boundary conditions are imposed in the z-direction to model infinitely long nanopillars. Since nanospheres require significantly more atoms than nanopillars for the same diameter, a spherical configuration is not considered in the present work. Since the stresses and deformation arise from the curved reaction front during lithiation, the current methods and conclusions are applicable to both nanopillars and nanospheres.

The effect that Li-ion insertion has on SiNPs is studied by using atomistic simulations with the open-source software LAMMPS.[38] The atomic interactions between the Li and Si atoms are described by the second nearest-neighbor modified embedded atom method (2NN MEAM) interatomic potential,[39] which has been used to predict the mechanical properties of both crystalline and amorphous Li_xSi alloys such as the elastic modulus, yield strength,[39] Li-ion diffusion,[40,41] and fracture mechanisms of lithiated Si.[24,42] The ReaxFF potential is not used because of its high computational cost. All simulation results are visualized by OVITO software.[43] The von Mises local shear strain is used to track the deformation history of the Li_xSi alloy during lithiation[44] (see Section 3 in the Supporting Information for its definition).

2.2. Lithiation Process. The lithiation process involves the slow diffusion of Li-ions in the Si and the Li−Si reaction at the Si/Li_xSi interface, which is beyond the timescale of conventional MD simulations.[45] Since the purpose of this work is to capture the stress and deformation of Li_xSi alloys and Si during the lithiation process, the real lithiation process is replaced and realized by a more efficient approach based on the existing experimental observations and simulation works. In this work, therefore, Li atoms are inserted into the predefined regions of SiNPs layer by layer as shown in Figure 2. The detailed predefined lithiation profiles are given in Figure S1. Each Si layer has a thickness of 1.0 nm because experiments have shown that the thickness of the Si/Li_xSi interface is around 1.0 nm.[6] For a SiNP with R_0 = 30.0 nm, therefore, 30 steps are required to realize full lithiation.

For a-SiNPs, since experiments have captured that lithiation is isotropic,[46] the Li_xSi−Si interfaces are taken to have a circular shape

https://doi.org/10.1021/acsami.1c02977
ACS Appl. Mater. Interfaces 2021, 13, 21310−21319

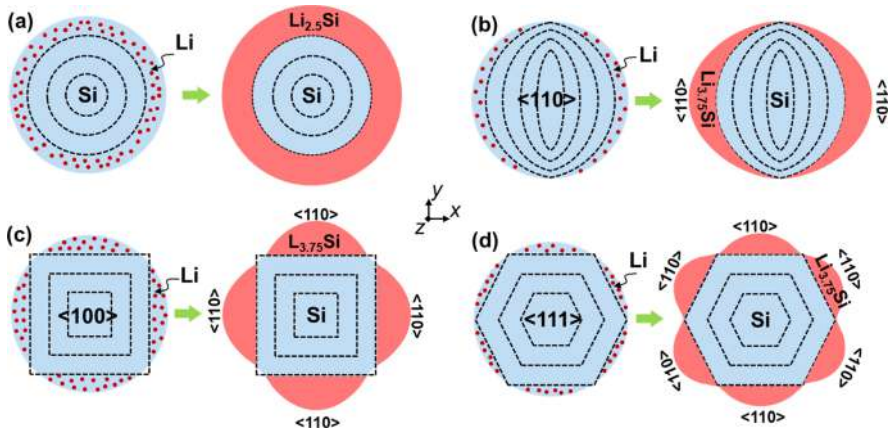

Figure 2. Lithiation protocol for different SiNPs. (a) a-SiNPs and (b–d) c-SiNPs with different axial orientations.

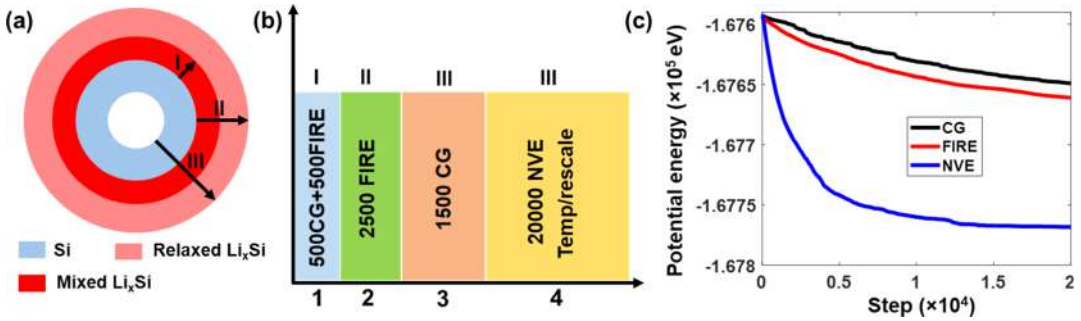

Figure 3. Energy minimization strategy used during lithiation of SiNPs. (a) Three regions defined in a lithiated SiNP; (b) schematic diagram for four-stage minimization; and (c) variation of potential energy using four different minimization methods during the fourth stage.

(Figure 2a). For the Li content x, we use x = 2.5 for a-SiNPs because previous experimental works have shown that only the formation of $Li_{2.5}Si$ alloys by two-phase lithiation can induce fracture, while further lithiation from $Li_{2.5}Si$ to $Li_{3.75}Si$ by one-phase lithiation has no effect.[18] In our simulations, we use x = 3.75 for c-SiNPs because experiments showed that $Li_{3.75}Si$ alloys form by two-phase lithiation, when lithiation starts from x = 0. The profiles of the concentration in the lithiation layer for c-SiNPs are approximately obtained from experimental images[47] or first-principles calculations,[48] as shown in Figure 2b–d (see Figure S1 for details). The exact Li-ion concentration profiles which can be obtained by solving an anisotropic diffusion problem will be considered in future work. For c-SiNPs, previous experimental and computational works showed that the energy barrier for the lithiation of Si is the lowest along the ⟨110⟩ direction, such that Li atoms diffuse into the Si crystal mostly along the ⟨110⟩ direction but rarely along the other lateral directions (swelling in the ⟨110⟩ direction during lithiation is about 9 times that in the ⟨111⟩ direction).[5,6,49] Structural relaxation is then performed to relax the lithiated SiNPs layer by layer.

3. NEW STRUCTURAL RELAXATION APPROACH

After Li atoms are inserted into the Si anodes manually within the simulation, the deformation of the lithiated SiNP is determined by structural relaxation, which is realized by performing energy minimization. The minimization method employed is of great importance for the efficiency and fidelity of the atomistic simulation results.[50] In accordance with experimental observations, three different regions need to be defined as seen in Figure 3a: region I corresponds to the newly formed Li_xSi alloy; region II corresponds to the total Li_xSi alloy present; and region III denotes the whole SiNP containing both the lithiated and unlithiated phases. Here, we propose a four-stage minimization strategy as shown in Figure 3b. The minimization is performed sequentially as follows: in the first minimization stage, only region I is relaxed by 500 steps using the CG method and 500 steps using the FIRE method,[51] while other regions are fixed. In the second stage, only region II is relaxed with 2500 steps using the FIRE method, while the other regions are fixed. In the third stage, the whole lithiated SiNP is relaxed by 1500 steps using the CG method. Some regions are fixed during the first two relaxation stages in order to avoid the unphysical deformation of these regions due to the extra-large repulsive forces in unrelaxed Li_xSi alloys, which is very important for the simulations of hollow a-SiNPs because the large repulsive forces could cause unphysical deformation of the inner surface. The CG and FIRE methods are adopted first because they are stable and robust, allowing to relax the very ill-conditioned structures.

In the fourth stage, different methods are tested to further relax the whole lithiated SiNP as seen in Figure 3c. As an example case, the a-SiNP with R_0 = 10.0 nm is considered. We first employ the CG method and the FIRE method using the Euler explicit integrator (the most efficient integrator in the FIRE method[50,52]). It is shown that the FIRE method can further decrease the system's energy compared to the CG method, but neither curve could reach a stable stage, indicating that the SiNP is not fully relaxed. Since the MEAM potential is computationally expensive, it is not feasible to use the CG or the FIRE methods to further relax the system, especially when it is large. Interestingly, we find that a dynamic relaxation method using *NVE* with temperature control (1 K) could be a very efficient tool to relax the lithiated SiNP as shown in Figure 3c. The *NVE* relaxation can be realized by the LAMMPS commands "fix nve/limit" and "fix temp/rescale". It is seen that

https://doi.org/10.1021/acsami.1c02977
ACS Appl. Mater. Interfaces 2021, 13, 21310–21319

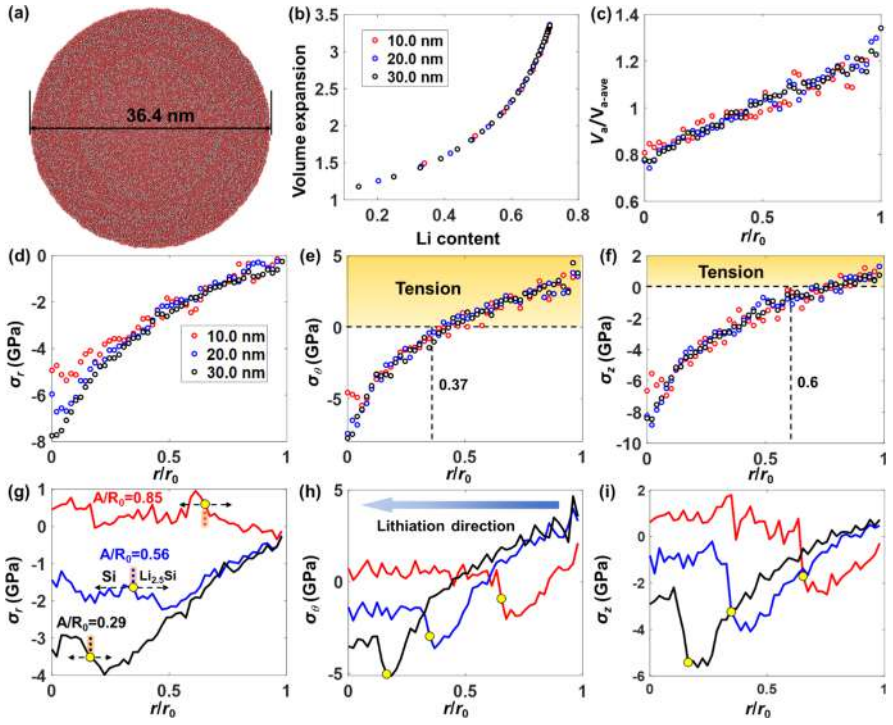

Figure 4. Simulation results of solid a-SiNPs with different diameters. (a) Final shape of a lithiated a-SiNP with an initial radius of 10.0 nm; (b) variation of volume expansion of a-SiNP with respect to Li content; (c–f) distribution of dimensionless atomic volume, atomic radial stress (σ_r), hoop stress (σ_θ), and axial stress (σ_z) after full lithiation along the dimensionless radial distance; and (g–i) stress distribution at different lithiation stages.

the system's energy decreases to a lower value quickly compared with the CG and FIRE methods and stops decreasing after 15,000 steps, indicating that the system is fully relaxed. Figure S2 presents the final shapes of all SiNPs after full lithiation with and without the fourth stage. It is seen that the structural relaxation in the fourth stage is indispensable for determining the morphologies of c-SiNPs, which agrees with the conclusions of a previous continuum-scale chemomechanical model.[53] Therefore, we perform 20,000 steps of *NVE* dynamic relaxation in stage four for all simulations as shown in Figure 3b. Note that the *NVE* relaxation can be performed under non-zero temperatures, indicating that our new method is also applicable to simulations at finite temperatures. The temperature effect on the deformation of SiNPs during lithiation will be considered in our future work.

It is noteworthy that the CG and FIRE methods are less efficient than *NVE* dynamic relaxation with temperature control in the present simulations, which completely differs from previous reports. Recent studies have shown that the FIRE method with the Euler explicit integrator is much faster than the CG method and other damped dynamic methods for relaxing nanostructures with free surfaces and dislocation cores.[50,52] The reason is that during minimization, the CG and FIRE methods were restricted by the energy change or power change, while *NVE* had no restriction. For the relaxation of nanostructures with free surfaces and dislocation cores, the initial configurations were close to equilibrium, and the energy profiles were complicated but the energy changes were small, such that carefully exploring the energy profile could accelerate the minimization process in the CG and FIRE methods. In the relaxation of the Li_xSi alloy, however, the initial energy is very high because the atomic distance was close, and the initial configuration was far away from the equilibrium state. Without restriction, *NVE* dynamic relaxation could efficiently decrease the system's energy by skipping the states with a small gradient or the minimal local states. Therefore, it can be concluded that the CG and FIRE methods are more efficient for fine energy minimization, while the *NVE* dynamic relaxation is better for coarse energy minimization with a significant energy change. Note that the lithiated SiNPs in previous MD works were only relaxed by the CG method,[32,33] possibly leading to the inconsistent stress distribution compared with theoretical predictions.[17]

4. DEFORMATION AND STRESS EVOLUTION DURING LITHIATION

4.1. Solid a-SiNPs. Figure 4a presents the final shape of an a-SiNP with an initial radius of 10.0 nm after complete lithiation. It is seen that lithiation resulted in a significant volume expansion as the diameter increased from 20.0 to 36.4 nm (336% volume expansion). Figure 4b–f shows the volume expansion, atomic volume, and stress distribution of a-SiNPs with different initial radii; the atomic volume is normalized by its average value. It is seen that the volume expansion increases with the Li content (Figure 4b). The maximum volume expansion is 336% after full lithiation for all a-SiNPs, regardless of their size, which is in good agreement with previous experiments[54] and diffusive MD simulations.[55] The atomic volume shows a gradient distribution as shown in Figure 4c. Specifically, upon maximum lithiation, the volume of the inner atoms is smaller than that of the outer atoms, indicative of the compressive stress in the center of the a-SiNPs. Figure 4d–f shows the distribution of the hoop stress (stress component in the tangential direction), radial stress (stress component toward or away from the central axis of SiNPs), and axial

https://doi.org/10.1021/acsami.1c02977
ACS Appl. Mater. Interfaces 2021, 13, 21310–21319

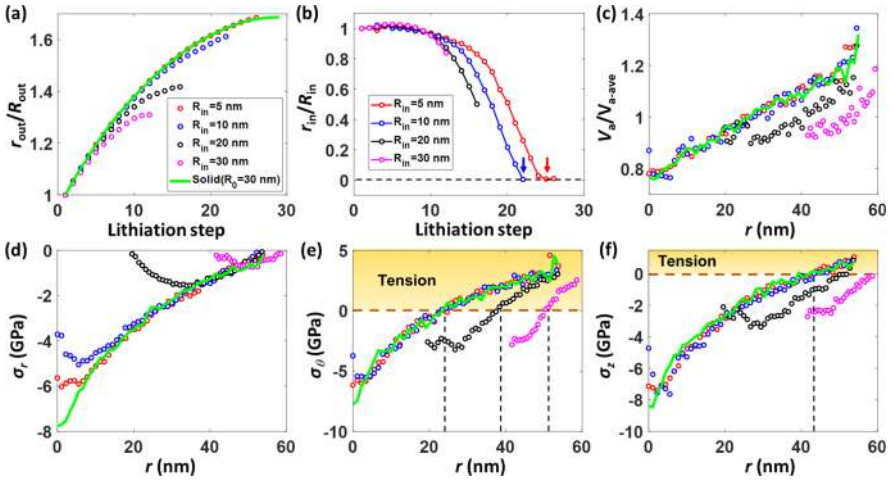

Figure 5. Simulation results of hollow a-SiNPs with different R_{in}. (a,b) Variation of R_{out} and R_{in} during the lithiation process. (c–f) Distribution of the atomic volume, atomic radial stress, hoop stress, and axial stress after full lithiation.

stress (stress component parallel to the axis of SiNPs) after full lithiation. The stress transformation from the Cartesian (x, y, z) coordinate system into the cylindrical (r, θ, z) coordinate system is given in Section 3 of the Supporting Information. Since atomic quantities are discrete, it is necessary to smooth the data spatially by taking the average in 100 × 100 bins for all SiNPs. An example is given in Figure S3 for an a-SiNP with R_0 = 30.0 nm.

In Figure 4e,f, it is seen that there exists a significant transition for the hoop stress (σ_θ) and axial stress (σz) from compressive to tensile at r_1/r_0 = 0.37 and r_2/r_0 = 0.6 for all a-SiNPs, respectively. Since a tensile stress is required for cracks to initiate and grow, this observation suggests that cracking occurs at the outer surface. This is consistent with recent phase-field modeling,[56] theoretical predictions,[17] and experimental observations, which show that cracks initiated from the outer particle surface upon lithiation.[47] The radial stress (σ_r), however, was always negative, indicative of the compressive state along the radial direction. Despite this transition in the hoop/axial stress, no cracks were observed in our MDs since the experiments have shown that the critical size for which fracture does not occur is below 180 nm in radius for c-SiNPs.[47] On the other hand, all simulated curves in Figure 4 are smooth and size-independent, indicating that the proposed structural relaxation approach in Section 3 is robust and effective.

Figure 4a–f indicates that SiNPs experience huge irreversible plastic deformation during lithiation. Since plastic deformation is often path-dependent, it is important to illustrate the lithiation-induced stress field at different stages. Figure 4g–i plots the distribution of three stress components at three lithiation stages (A/R_0 = 0.85, 0.56, and 0.29) for an a-SiNP with R_0 = 30 nm. Yellow circles indicate the position up to which lithiation has taken place. Curves before the yellow circles correspond to the stress field in the unlithiated Si core, whereas curves after the yellow circles correspond to the stress field in the lithiated shell. It is seen that all stress components are constant and negative (compressive) in the unlithiated Si core and decrease as lithiation continues. In the lithiated Si shell, the radial stress (σ_r) is close to zero in the early stages of lithiation and decreases gradually along the radial direction of the a-SiNP as lithiation continues. The hoop stress (σ_θ) and axial stress (σ_z) gradually increase and become tensile due to the "pushing-out" effect. These results agree well with previous theoretical predictions.[17,18]

4.2. Hollow a-SiNPs. Figure 5a,b summarizes the change in the radii of all hollow a-SiNPs during lithiation (normalized by the initial dimensions), and Figure 5c–f gives the distribution of different quantities along the radial direction after full lithiation. The simulation results of the solid a-SiNP with R_0 = 30.0 nm are also plotted for comparison purposes. During lithiation, r_{out}/R_{out} increases gradually and coincides with that of solid a-SiNPs for all hollow a-SiNPs at the early stages of lithiation as shown in Figure 5a, indicating that lithiation-induced deformation is initially independent of the hole size (R_{in}). Of particular interest is that the initial outer radii of hollow a-SiNPs with R_{in} = 5.0, 10.0, and 20.0 nm are larger than that of the solid a-SiNP before lithiation, but the final radii of these a-SiNPs are similar to that of the solid ones after lithiation as shown in Figure S4. The plot in Figure 5b shows that r_{in} remains constant initially but decreases in the later lithiation steps. Two hollow a-SiNPs with R_{in} = 5.0 and 10.0 nm have zero inner radii after lithiation as indicated by arrows, showing that the inner holes are completely closed due to the inward volume expansion. It should be noted that previous experiments showed no inward expansion in lithiated Si nanotubes.[8] The discrepancy between our simulations and experiments can be attributed to the absence of native oxides herein. In experiments, the native SiO_x coating that was present at the inner surface could prohibit inward expansion. Figure 5c shows that the hollow a-SiNPs with R_{in} = 5.0 and 10.0 nm and the solid a-SiNP in Section 4.1 undergo a similar atomic volume expansion, but the hollow a-SiNPs with R_{in} = 20.0 and 30.0 nm experience a smaller atomic volume expansion upon maximum lithiation and exhibit a size effect: the bigger the R_{in}, the smaller the atomic volume expansion. Similarly, Figure 5d–f shows that the stresses in the hollow a-SiNPs with R_{in} = 5.0 and 10.0 nm are similar to those in the solid a-SiNP, but for the hollow a-SiNPs with R_{in} = 20.0 and 30.0 nm, they are different. Particularly, when R_{in} = 20.0 and 30.0 nm, the hollow a-SiNPs have a zero radial stress near the inner surface (Figure 5d). A pronounced size effect can be observed in Figure 5e,f: the bigger the R_{in}, the smaller the hoop stress and axial stress, and thinner the $Li_{2.5}Si$ alloy region under tension, which is in good agreement with the theoretical predictions for hoop stresses.[57]

https://doi.org/10.1021/acsami.1c02977
ACS Appl. Mater. Interfaces 2021, 13, 21310–21319

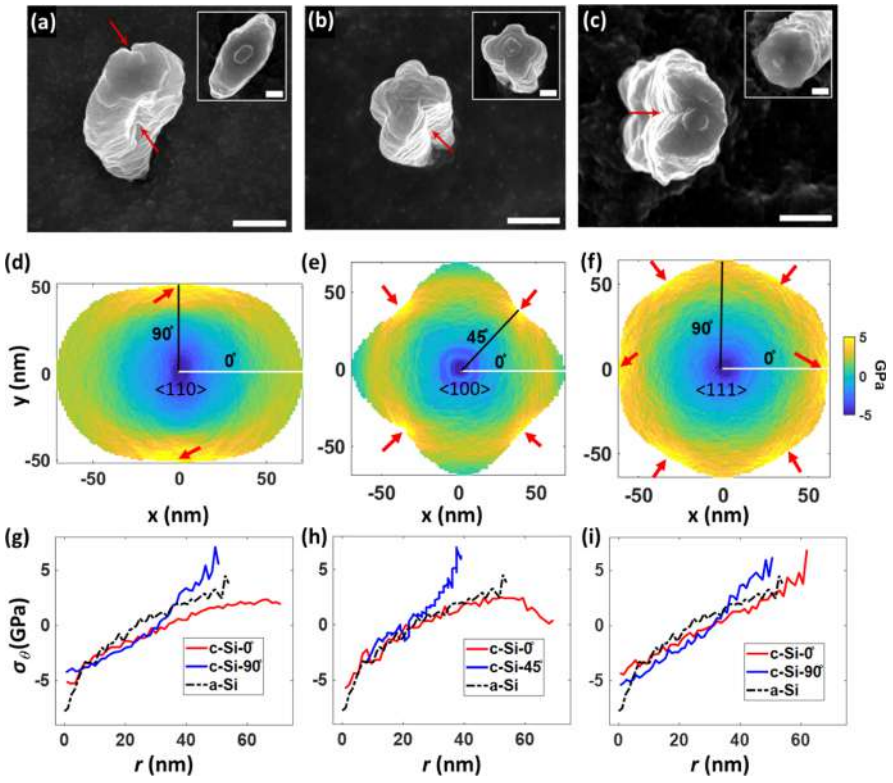

Figure 6. Experimental images and simulation results of c-SiNPs with different axial orientations after lithiation. (a–c) Top-view SEM images of c-SiNPs of each crystal orientation (⟨110⟩, ⟨100⟩, and ⟨111⟩) after lithiation.[47] The scale bars in the main images are 500 nm, and the scale bars in the insets are 200 nm. Reproduced with permission from ref 47. (d–f) Deformed shapes and hoop stress distribution in the whole region of c-SiNPs with axial orientations of ⟨110⟩, ⟨100⟩, and ⟨111⟩. (g–i) Hoop stress distribution in particular directions.

We have shown that the hollow a-SiNPs with a small R_{in} and the solid nanopillar have similar deformation (Figure 5a), distributions of the atomic volume (Figure 5c), and stresses (Figure 5d–f) after full lithiation, indicating that these hollow a-SiNPs are irreversibly transformed to solid ones by closing the inner holes, due to the expansion upon lithiation. In designing hollow nanopillars, therefore, a bigger R_{in} is necessary. On the other hand, the Li diffusion distance is smaller for the hollow nanopillar with a bigger R_{out} (because R_{in} and R_{out} were changed in a way to keep the volume constant), leading to a higher rate capability due to the shorter time required to complete lithiation, which is consistent with existing experimental observations.[57] Previous theoretical work also showed that hollow a-SiNPs could be fully lithiated with a lower stress-induced barrier than solid a-SiNPs.[17] Another advantage of hollow a-SiNPs is that although the hollow a-SiNPs are bigger than the solid a-SiNPs before lithiation, they attain a similar size after lithiation, especially when R_{in} = 20 nm for which the inner hole is retained, such that the hollow a-SiNP can be stored in the same volume as the solid a-SiNP can after lithiation. More importantly, the hollow a-SiNPs have better mechanical durability against fracture than the solid a-SiNP, which will be discussed in Section 6.

It should be noted that for Si nanopillars, Li diffusion may occur from both inner and outer surfaces, which can be simulated using our method by inserting Li atoms from the inner and outer surfaces and performing structural relaxation. Herein, we consider lithiation from the outer surface only as this is how lithiation occurs in hollow Si spheres, which are more promising for commercial use, and we wanted our simulations to provide insight into the deformation of such configurations.

4.3. Solid c-SiNPs. Figure 6 presents the simulation results of three solid c-SiNPs with different axial orientations ⟨110⟩, ⟨100⟩, and ⟨111⟩. It is seen that the anisotropic volume expansions, which arise from the orientation-dependent lithiation rate specified in Figure 2, are successfully captured for all c-SiNPs (Figure 6d–f) as they are in agreement with the corresponding experimental images as shown in Figure 6a–c.[47] Since the ⟨110⟩ c-SiNP, the ⟨100⟩ c-SiNP, and the ⟨111⟩ c-SiNP have two, four, and six ⟨110⟩ lateral directions, respectively, they expand into ellipse, cross, and hexagonal shapes, respectively. The volume expansions are calculated as 450% for the three c-SiNP shapes. The particular locations that have the higher hoop stress indicated by red arrows in Figure 6d–f are between neighboring ⟨110⟩ directions, which are consistent with the preferred crack initiation positions observed in Figure 6a–c. The hoop stress distribution along different directions is extracted and plotted in Figure 6d–f. For all c-SiNPs, the hoop stresses show a transition from compressive to tensile but depend on the direction due to the anisotropic lithiation. For the ⟨110⟩ c-SiNP, for example, the hoop stress along the 90° direction is higher than that of a-Si when r > 40.0 nm, whereas the hoop stress along 0° is lower. Similarly, the ⟨100⟩ c-SiNP and the ⟨111⟩ c-SiNP experience a higher hoop stress along the 45° direction and the 90° direction, respectively, when compared to the a-SiNP.

5. PLASTIC FLOW OF LITHIATED SINPS

Although the present MD simulations cannot capture crack initiation and propagation as the SiNPs considered are small,

https://doi.org/10.1021/acsami.1c02977
ACS Appl. Mater. Interfaces 2021, 13, 21310–21319

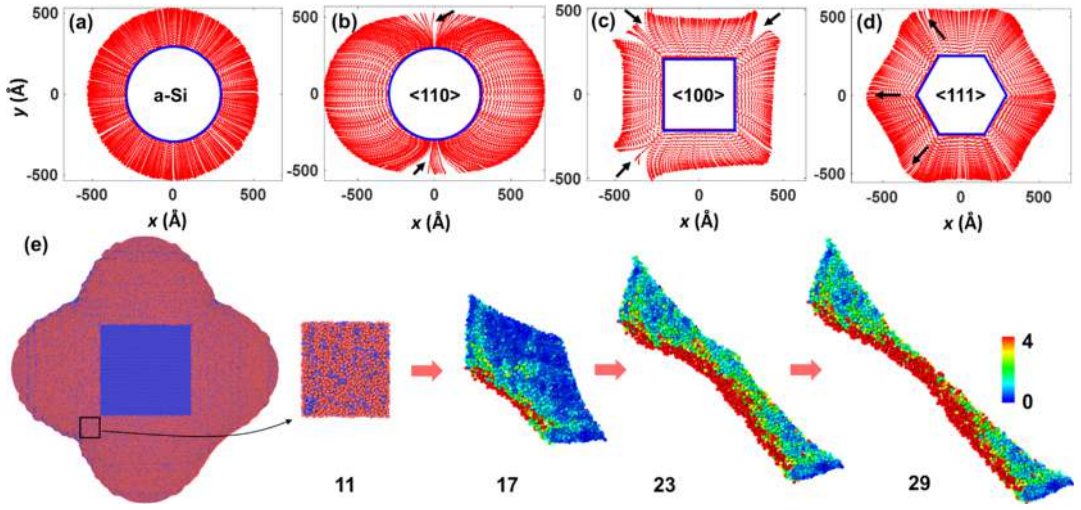

Figure 7. Plastic flow in c-SiNP. (a–d) Trajectories of selected atoms in c-SiNPs. (e) Atomic shear strain of a deformed $Li_{3.75}Si$ alloy block at different lithiation stages. 11, 17, 23, and 29 denote lithiation steps.

we illustrate the large plastic deformation required to accommodate the huge lithiation-induced mechanical stress in Figure 7. Figure 7a–d shows the trajectories of selected Si atoms (represented by blue lines initially) during lithiation for a solid a-SiNP and three c-SiNPs with different axial orientations. According to the lithiation profiles in Figure 2, the selected Si atoms are in a circular shape for the a-SiNP and ⟨110⟩ c-SiNP, in a square shape for the ⟨100⟩ c-SiNP, and in a hexagonal shape for the ⟨111⟩ c-SiNP. It is seen that the a-SiNP deforms homogeneously along all directions. The c-SiNPs, however, show significant anisotropic plastic flow (Figure 7a). In particular, the ⟨110⟩ c-SiNP deforms along only two lateral ⟨110⟩ directions such that the top and bottom of the SiNP experience large deformation (Figure 7b). For the ⟨100⟩ c-SiNP, the generated $Li_{3.75}Si$ alloys expand along four lateral ⟨110⟩ directions, such that four corners of the square experience large deformation incompatibility (Figure 7c). Similarly, the ⟨111⟩ c-SiNP deforms along six lateral ⟨110⟩ directions and the six corners of the hexagon deform (Figure 7d). These results indicate that the ⟨111⟩ c-SiNP has a better fracture resistance because the deformation can be shared in more directions instead of being accumulated, which can be further confirmed by the smaller discontinuities pointed out by arrows in Figure 7d and the lower maximum hoop stress in Figure 6i. Previous experiments showed that c-SiNPs, with approximately the same size (inset of Figure 6b) as our simulations, that had the ⟨100⟩ orientation fractured, whereas those with the ⟨111⟩ orientation deformed symmetrically in a hexagonal shape[5] (inset of Figure 6c).

Note that the discontinuities in Figure 7b,c only indicate that the initially adjacent Si atoms are separated by plastic flow rather than by fracture. In order to better elucidate the plastic flow that induces Si atom separation at the atomic scale, a group of $Li_{3.75}Si$ atoms in a squared region is marked and tracked during lithiation, and the deformed shapes are presented in Figure 7e. All atoms are colored by the atomic shear strain to illustrate inelastic deformation. It is seen that the initial square is smoothly deformed as a long strip and the inelastic (plastic) deformation concentrates on the lower side of the strip, which accounts for the discontinuities in Figure 7c, while other regions deform significantly by activating shear transformation zones (STZs). These results agree well with the high damage tolerance of lithiated Si captured in the previous experiments.[30]

6. FRACTURE ANALYSIS OF SI NANOPILLARS DUE TO LITHIATION

Although crack initiation and propagation were not captured in Section 4 due to the small pillar sizes, our simulation results can be used to analyze the fracture of Si nanopillars due to lithiation. It is known that the stress intensity factor (K_I) in fracture mechanics can be expressed as a function of the applied stress (σ) and the critical crack length (a_c)

$$K_I = \beta\sigma\sqrt{\pi a_c} \tag{1}$$

The critical value of K_I is defined as the fracture toughness (K_{Ic}) of the materials, which is used to quantify a material's resistance to crack propagation. To simplify the analysis, it is assumed that the stress intensity modification factor (β) which accounts for the geometry is very close to 1 for all SiNPs. We recognize that eq 1 has been deduced from an infinitely long plate, but it can give a good estimation for SiNPs. In the following analysis, it is shown that the theoretical results predicted by eq 1 qualitatively agree with previous experimental results, indicating that these assumptions are acceptable. To obtain the critical radius of the SiNP that will fracture due to lithiation, we assume that the critical crack length equals the thickness (t) of Li_xSi under tension. In Figure 4e, it is seen that $t = \alpha r_0$, where $\alpha$is a size-independent parameter 0.63. In Figure 4b, we have $\pi r_0^2 = 3.36\pi R_0^2$, such that $r_0 = 1.83R_0$, which is a size-independent relationship. Substituting these relationships in eq 1, we can get the critical radius at which a SiNP will fracture by

$$R_{0c} = \frac{1}{1.15\pi}\left(\frac{K_{Ic}}{\sigma}\right)^2 \tag{2}$$

Taking $K_{Ic} = 4.62\ \text{MPa}\sqrt{m}$[30] and $\sigma_\theta = 3.8$ GPa (Figure 4e) for $Li_{2.5}Si$, we find a critical radius of $R_{0c} = 409.1$ nm for the a-SiNP. Although experimental data for a-SiNPs is not available, we find that this prediction agrees well with the experimental values of 435.0 nm for a-Si nanoparticles.[58] By taking $K_{Ic} = 7.12\ \text{MPa}\sqrt{m}$[30] and $\sigma_\theta = 7.1$ GPa (Figure 6h) for $Li_{3.75}Si$ and using a similar fracture model, the critical radius can be found

https://doi.org/10.1021/acsami.1c02977
ACS Appl. Mater. Interfaces 2021, 13, 21310–21319

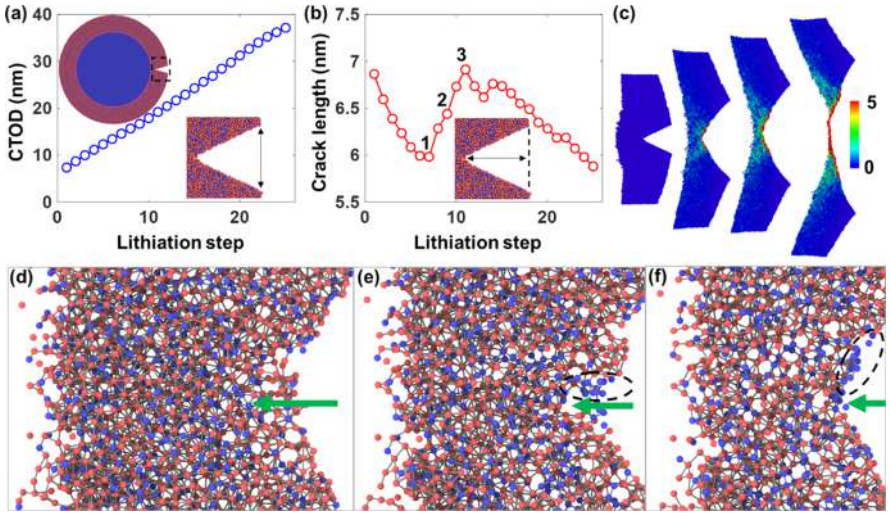

Figure 8. Simulation results of lithiation in a solid a-SiNP with R_{in} = 30.0 nm after inserting a crack. (a,b) Variation of CTOD and crack length during lithiation. (c) Atomic shear strain at the crack tip during lithiation. (d–f) Atomic bonds at the crack tip at points 1–3 in (b).

as 278.4 nm for c-SiNPs, which is larger than the reported value of 180.0 nm in experiments[47] as they experience anisotropic lithiation. However, the comparable magnitude between eq 2 and experiments indicates that this simple fracture model can be used to guide the design of Si anodes. Based on eqs 1 and 2, we define the factor of safety or fracture resistance (n) as

$$n = \frac{K_{Ic}}{K_I} = \frac{K_{Ic}}{\sigma\sqrt{1.15\pi R_0}} \tag{3}$$

which is a function of stress (σ) and size (R_0). The higher the value of n, the better the mechanical durability against lithiation-induced fracture. First, the smaller the R_0, the higher the n, which explains why nanostructured Si anodes are mechanically more stable. Second, when R_0 = 30.0 nm, n(a-SiNP) = 3.69 and n(c-SiNP) = 3.09, such that c-SiNPs are easier to fracture during lithiation. Third, when the inner holes are not closed, the hollow a-SiNPs with the larger R_{in} experience lower tensile stresses as shown in Figure 5e,f, such that hollow a-SiNPs have a higher n than solid a-SiNPs, which is consistent with previous experiments[20,57] and chemomechanical modeling results that showed higher mechanical stability for hollow SiNPs.[20] Based on this crude approximation, a hollow a-SiNP is the preferred anode design.

In order to investigate the fracture process in a SiNP during lithiation, a crack with an initial length of 7.0 nm is inserted at the outer surface of a solid a-SiNP with R_0 = 30.0 nm as shown in the upper inset of Figure 8. Then, lithiation is performed as already described in Section 2 but with a preexisting crack present. The crack tip opening displacement (CTOD) and crack length during lithiation are plotted in Figure 8a,b, respectively. It is seen that although the CTOD continuously increases as the lithiation front advances, the crack length decreases, indicating that the crack is blunt and the deformation near the crack tip is dominated by plastic flow. The atomic shear strain of the crack tip shown in Figure 8c indicates that the deformation due to the crack opening is consumed by forming STZs or shear bands. Interestingly, the crack length increases from points 1–3 in Figure 8b, suggesting a temporary crack propagation. Figure 8d–f presents the atomic bonds near the crack tip at points 1–3. It is seen that crack propagation results from Li–Si bonds breaking near a Si-rich region and forming a cavity (Figure 8d,e). After propagation, the Si atoms in this region are attracted to the upper surface of the crack (Figure 8f). Previous work has shown that the surrounding Li atoms play a crucial role in accommodating the lithiation-induced deformation by the Li–Li and Li–Si bond switching process in $Li_{2.5}Si$ alloys.[30] For the Si-rich region in Figure 8, such a bond switching process is inhibited because fewer Li atoms are present. This Si-rich-induced crack propagation results from the non-perfect Li insertion approach presented in Section 2.2 because all atoms could move during lithiation, but lithiation profiles are defined before simulation as shown in Figure 2. This imperfection can be improved in future work.

The crack propagation in Si-rich regions in Figure 8 can be used to explain the discrepancy of the critical fracture radii obtained between eq 2 and experiments for c-SiNPs. In-situ experiments have shown that some preexisting defects such as twin boundaries remained in the c-Si core during lithiation.[59] These defects could induce high local stresses near the defects upon lithiation as shown in Figure S5. The defects in c-SiNPs could be voids, dislocations, grain boundaries, or any non-perfect lattice position that can induce an inhomogeneous stress distribution during lithiation. Moreover, previous experiments and MD simulations have shown that external stresses significantly affect the lithiation rate.[26,27,31] In particular, tensile stresses accelerate the lithiation rate, while compressive stresses retard it. Consequently, the high local stress near the defects can induce inhomogeneous lithiation and a non-uniform Si distribution. The Si-rich regions are more brittle by forming cavitation during lithiation as presented in Figure 8d–f, which can lead to the lower fracture resistance observed for c-SiNPs experimentally. For a-SiNPs, however, lithiation is more homogeneous due to the absence of defects in the a-Si core, such that a-SiNPs have better mechanical durability.

7. CONCLUSIONS

Our results show the significant insight that MD simulations can provide in understanding the mechanical effects of lithiation in SiNPs. First, we showed that the *NVE* dynamic relaxation with temperature control could better relax the

https://doi.org/10.1021/acsami.1c02977
ACS Appl. Mater. Interfaces 2021, 13, 21310–21319

lithiated Li_xSi alloys than the CG and FIRE methods, which provides a valuable tool to study LIBs and other batteries atomistically. The case study we chose to examine is that of crystalline and amorphous SiNPs with different axial orientations via large-scale atomistic simulations, allowing us to capture at the atomic scale for the first time the lithiation-induced hoop stress, radial stress, and axial stress. Particularly we showed the transition of the hoop stress and axial stress from compressive to tensile, which can explain the experimental observations that cracks initiated from the outer surfaces of the SiNPs. Most importantly, the formation of plastic flow during lithiation was revealed for the first time by tracking the trajectories of selected Si atoms and the atomic shear strain of the selected $Li_{3.75}Si$ region showing the high damage tolerance of lithiated Si by forming shear bands. Finally, based on the simulation results, a simple fracture mechanics model was successfully used to predict the critical size of SiNPs that will fracture and quantify the fracture resistance of various SiNPs. Our novel crack propagation simulation suggests that pre-existing defects in c-SiNPs could aggravate crack nucleation and propagation in Si-rich regions that arise from the stress-dependent lithiation near these defects. These findings can be used to guide the design of new Si anodes by tuning the geometry.

■ ASSOCIATED CONTENT

Supporting Information

The Supporting Information is available free of charge at https://pubs.acs.org/doi/10.1021/acsami.1c02977.

Predefined lithiation layers for all Si nanopillars; morphologies of Si nanopillars after full lithiation with and without *NVE* relaxation; atomic stress calculation; and stress distribution near dislocations during lithiation (PDF)

■ AUTHOR INFORMATION

Corresponding Author

Katerina E. Aifantis − *Department of Mechanical and Aerospace Engineering, University of Florida, Gainesville, Florida 32611, United States;* orcid.org/0000-0002-0105-548X; Phone: (352) 392-6227; Email: kaifantis@ufl.edu

Author

Fei Shuang − *Department of Mechanical and Aerospace Engineering, University of Florida, Gainesville, Florida 32611, United States*

Complete contact information is available at: https://pubs.acs.org/10.1021/acsami.1c02977

Author Contributions

F.S.: writing—original draft, methodology, conceptualization, and formal analysis. K.E.A.: writing—original draft, conceptualization, methodology, formal analysis, and funding acquisition.

Notes

The authors declare no competing financial interest.

■ ACKNOWLEDGMENTS

The authors are grateful to the National Science Foundation for supporting this work through the CMMI grant (CMMI-1762602).

■ REFERENCES

(1) Whittingham, M. S. Materials Challenges Facing Electrical Energy Storage. *MRS Bull.* **2008**, *33*, 411−419.

(2) Boukamp, B. A.; Lesh, G. C.; Huggins, R. A. All-Solid Lithium Electrodes with Mixed-Conductor Matrix. *J. Electrochem. Soc.* **1981**, *128*, 725−729.

(3) Kasavajjula, U.; Wang, C.; Appleby, A. J. Nano- and bulk-silicon-based insertion anodes for lithium-ion secondary cells. *J. Power Sources* **2007**, *163*, 1003−1039.

(4) Beaulieu, L. Y.; Eberman, K. W.; Turner, R. L.; Krause, L. J.; Dahn, J. R. Colossal Reversible Volume Changes in Lithium Alloys. *Electrochem. Solid-State Lett.* **2001**, *4*, A137.

(5) Lee, S. W.; McDowell, M. T.; Choi, J. W.; Cui, Y. Anomalous Shape Changes of Silicon Nanopillars by Electrochemical Lithiation. *Nano Lett.* **2011**, *11*, 3034−3039.

(6) Liu, X. H.; Wang, J. W.; Huang, S.; Fan, F.; Huang, X.; Liu, Y.; Krylyuk, S.; Yoo, J.; Dayeh, S. A.; Davydov, A. V.; Mao, S. X.; Picraux, S. T.; Zhang, S.; Li, J.; Zhu, T.; Huang, J. Y. In Situ Atomic-Scale Imaging of Electrochemical Lithiation in Silicon. *Nat. Nanotechnol.* **2012**, *7*, 749−756.

(7) Li, Y.; Yan, K.; Lee, H. W.; Lu, Z.; Liu, N.; Cui, Y. Growth of Conformal Graphene Cages on Micrometre-Sized Silicon Particles as Stable Battery Anodes. *Nat. Energy* **2016**, *1*, 15029.

(8) Wang, J.; Luo, H.; Liu, Y.; He, Y.; Fan, F.; Zhang, Z.; Mao, S. X.; Wang, C.; Zhu, T. Tuning the Outward to Inward Swelling in Lithiated Silicon Nanotubes via Surface Oxide Coating. *Nano Lett.* **2016**, *16*, 5815−5822.

(9) Zhang, X.-y.; Song, W.-L.; Liu, Z.; Chen, H.-S.; Li, T.; Wei, Y.; Fang, D.-n. Geometric Design of Micron-Sized Crystalline Silicon Anodes through: In Situ Observation of Deformation and Fracture Behaviors. *J. Mater. Chem. A* **2017**, *5*, 12793−12802.

(10) Aifantis, K.; Hackney, S. A. An ideal elasticity problem for li-batteries. *J. Mech. Phys. Solids* **2003**, *14*, 413−427.

(11) Aifantis, K. E.; Dempsey, J. P. Stable Crack Growth in Nanostructured Li-Batteries. *J. Power Sources* **2005**, *143*, 203−211.

(12) Aifantis, K. E.; Hackney, S. A.; Dempsey, J. P. Design Criteria for Nanostructured Li-Ion Batteries. *J. Power Sources* **2007**, *165*, 874−879.

(13) Hu, B.; Ma, Z.; Lei, W.; Zou, Y.; Lu, C. A chemo-mechanical model coupled with thermal effect on the hollow core−shell electrodes in lithium-ion batteries. *Theor. Appl. Mech. Lett.* **2017**, *7*, 199−206.

(14) Wu, H.; Xie, Z.; Wang, Y.; Zhang, P.; Sun, L.; Lu, C.; Ma, Z. A Constitutive Model Coupling Irradiation with Two-Phase Lithiation for Lithium-Ion Battery Electrodes. *Philos. Mag.* **2019**, *99*, 992−1013.

(15) Zhang, S.; Jiang, W.; Tonks, M. R. A New Phase Field Fracture Model for Brittle Materials That Accounts for Elastic Anisotropy. *Comput. Methods Appl. Mech. Eng.* **2020**, *358*, 112643.

(16) Zhang, P.; Ma, Z.; Wang, Y.; Zou, Y.; Sun, L.; Lu, C. Lithiation-Induced Interfacial Failure of Electrode-Collector: A First-Principles Study. *Mater. Chem. Phys.* **2019**, *222*, 193−199.

(17) Jia, Z.; Li, T. Stress-Modulated Driving Force for Lithiation Reaction in Hollow Nano-Anodes. *J. Power Sources* **2015**, *275*, 866−876.

(18) Jia, Z.; Li, T. Intrinsic Stress Mitigation via Elastic Softening during Two-Step Electrochemical Lithiation of Amorphous Silicon. *J. Mech. Phys. Solids* **2016**, *91*, 278−290.

(19) Wen, J.; Wei, Y.; Cheng, Y.-T. Stress Evolution in Elastic-Plastic Electrodes during Electrochemical Processes: A Numerical Method and Its Applications. *J. Mech. Phys. Solids* **2018**, *116*, 403−415.

(20) Wang, C.; Wen, J.; Luo, F.; Quan, B.; Li, H.; Wei, Y.; Gu, C.; Li, J. Anisotropic Expansion and Size-Dependent Fracture of Silicon Nanotubes during Lithiation. *J. Mater. Chem. A* **2019**, *7*, 15113−15122.

(21) Réthoré, J.; Zheng, H.; Li, H.; Li, J.; Aifantis, K. E. A Multiphysics Model That Can Capture Crack Patterns in Si Thin Films Based on Their Microstructure. *J. Power Sources* **2018**, *400*, 383−391.

(22) Hu, P.; Peng, W.; Wang, B.; Xiao, D.; Ahuja, U.; Réthoré, J.; Aifantis, K. E. Concentration-Gradient Prussian Blue Cathodes for Na-Ion Batteries. *ACS Energy Lett.* **2020**, *5*, 100−108.
(23) Fan, F.; Huang, S.; Yang, H.; Raju, M.; Datta, D.; Shenoy, V. B.; Van Duin, A. C. T.; Zhang, S.; Zhu, T. Mechanical Properties of Amorphous LixSi Alloys: A Reactive Force Field Study. *Modell. Simul. Mater. Sci. Eng.* **2013**, *21*, 074002.
(24) Ding, B.; Li, X.; Zhang, X.; Wu, H.; Xu, Z.; Gao, H. Brittle versus Ductile Fracture Mechanism Transition in Amorphous Lithiated Silicon: From Intrinsic Nanoscale Cavitation to Shear Banding. *Nano Energy* **2015**, *18*, 89−96.
(25) Khosrownejad, S. M.; Curtin, W. A. Crack Growth and Fracture Toughness of Amorphous Li-Si Anodes: Mechanisms and Role of Charging/Discharging Studied by Atomistic Simulations. *J. Mech. Phys. Solids* **2017**, *107*, 542−559.
(26) Pan, J.; Zhang, Q.; Li, J.; Beck, M. J.; Xiao, X.; Cheng, Y.-T. Effects of Stress on Lithium Transport in Amorphous Silicon Electrodes for Lithium-Ion Batteries. *Nano Energy* **2015**, *13*, 192−199.
(27) Ding, B.; Wu, H.; Xu, Z.; Li, X.; Gao, H. Stress Effects on Lithiation in Silicon. *Nano Energy* **2017**, *38*, 486−493.
(28) Kim, K. J.; Wortman, J.; Kim, S.-Y.; Qi, Y. Atomistic Simulation Derived Insight on the Irreversible Structural Changes of Si Electrode during Fast and Slow Delithiation. *Nano Lett.* **2017**, *17*, 4330−4338.
(29) Jung, H.; Lee, M.; Yeo, B. C.; Lee, K.-R.; Han, S. S. Atomistic Observation of the Lithiation and Delithiation Behaviors of Silicon Nanowires Using Reactive Molecular Dynamics Simulations. *J. Phys. Chem. C* **2015**, *119*, 3447−3455.
(30) Wang, X.; Fan, F.; Wang, J.; Wang, H.; Tao, S.; Yang, A.; Liu, Y.; Beng Chew, H.; Mao, S. X.; Zhu, T.; Xia, S. High Damage Tolerance of Electrochemically Lithiated Silicon. *Nat. Commun.* **2015**, *6*, 8417.
(31) Gu, M.; Yang, H.; Perea, D. E.; Zhang, J.-G.; Zhang, S.; Wang, C.-M. Bending-Induced Symmetry Breaking of Lithiation in Germanium Nanowires. *Nano Lett.* **2014**, *14*, 4622−4627.
(32) Fan, F.; Yang, H.; Zeng, Z. An Atomistic Perspective on Lithiation-Induced Stress in Silicon Nanopillars. *Scr. Mater.* **2018**, *152*, 74−78.
(33) Cao, L.; Yang, H.; Fan, F. Stress Generation during Anisotropic Lithiation in Silicon Nanopillar Electrodes: A Reactive Force Field Study. *Phys. Lett. A* **2019**, *383*, 125955.
(34) Zhao, K.; Pharr, M.; Wan, Q.; Wang, W. L.; Kaxiras, E.; Vlassak, J. J.; Suo, Z. Concurrent Reaction and Plasticity during Initial Lithiation of Crystalline Silicon in Lithium-Ion Batteries. *J. Electrochem. Soc.* **2012**, *159*, A238−A243.
(35) Kushima, A.; Huang, J. Y.; Li, J. Quantitative Fracture Strength and Plasticity Measurements of Lithiated Silicon Nanowires by in Situ TEM Tensile Experiments. *ACS Nano* **2012**, *6*, 9425−9432.
(36) Chang, L.; Lu, Y.; He, L.; Ni, Y. Phase Field Model for Two-Phase Lithiation in an Arbitrarily Shaped Elastoplastic Electrode Particle under Galvanostatic and Potentiostatic Operations. *Int. J. Solids Struct.* **2018**, *143*, 73−83.
(37) Chen, L.; Fan, F.; Hong, L.; Chen, J.; Ji, Y. Z.; Zhang, S. L.; Zhu, T.; Chen, L. Q. A Phase-Field Model Coupled with Large Elasto-Plastic Deformation: Application to Lithiated Silicon Electrodes. *J. Electrochem. Soc.* **2014**, *161*, F3164−F3172.
(38) Plimpton, S. Fast Parallel Algorithms for Short − Range Molecular Dynamics. *J. Comput. Phys.* **1995**, *117*, 1−19.
(39) Cui, Z.; Gao, F.; Cui, Z.; Qu, J. A Second Nearest-Neighbor Embedded Atom Method Interatomic Potential for Li-Si Alloys. *J. Power Sources* **2012**, *207*, 150−159.
(40) Wang, H.; Ji, X.; Chen, C.; Xu, K.; Miao, L. Lithium Diffusion in Silicon and Induced Structure Disorder: A Molecular Dynamics Study. *AIP Adv.* **2013**, *3*, 112102.
(41) Yan, X.; Gouissem, A.; Sharma, P. Atomistic Insights into Li-Ion Diffusion in Amorphous Silicon. *Mech. Mater.* **2015**, *91*, 306−312.
(42) Wang, H.; Chew, H. B. Molecular Dynamics Simulations of Plasticity and Cracking in Lithiated Silicon Electrodes. *Extrem. Mech. Lett.* **2016**, *9*, 503−513.
(43) Stukowski, A. Visualization and Analysis of Atomistic Simulation Data with OVITO-the Open Visualization Tool. *Modell. Simul. Mater. Sci. Eng.* **2010**, *18*, 015012.
(44) Shimizu, F.; Ogata, S.; Li, J. Theory of Shear Banding in Metallic Glasses and Molecular Dynamics Calculations. *Mater. Trans.* **2007**, *48*, 2923−2927.
(45) Lee, H.-S.; Lee, B.-J. Structural Changes during Lithiation and Delithiation of Si Anodes in Li-Ion Batteries: A Large Scale Molecular Dynamics Study. *Met. Mater. Int.* **2014**, *20*, 1003−1009.
(46) Wang, J. W.; He, Y.; Fan, F.; Liu, X. H.; Xia, S.; Liu, Y.; Harris, C. T.; Li, H.; Huang, J. Y.; Mao, S. X.; Zhu, T. Two-Phase Electrochemical Lithiation in Amorphous Silicon. *Nano Lett.* **2013**, *13*, 709−715.
(47) Lee, S. W.; McDowell, M. T.; Berla, L. A.; Nix, W. D.; Cui, Y. Fracture of Crystalline Silicon Nanopillars during Electrochemical Lithium Insertion. *Proc. Natl. Acad. Sci. U.S.A.* **2012**, *109*, 4080−4085.
(48) Cubuk, E. D.; Wang, W. L.; Zhao, K.; Vlassak, J. J.; Suo, Z.; Kaxiras, E. Morphological Evolution of Si Nanowires upon Lithiation: A First-Principles Multiscale Model. *Nano Lett.* **2013**, *13*, 2011−2015.
(49) Yang, H.; Fan, F.; Liang, W.; Guo, X.; Zhu, T.; Zhang, S. A Chemo-Mechanical Model of Lithiation in Silicon. *J. Mech. Phys. Solids* **2014**, *70*, 349−361.
(50) Shuang, F.; Xiao, P.; Shi, R.; Ke, F.; Bai, Y. Influence of Integration Formulations on the Performance of the Fast Inertial Relaxation Engine (FIRE) Method. *Comput. Mater. Sci.* **2019**, *156*, 135−141.
(51) Bitzek, E.; Koskinen, P.; Gähler, F.; Moseler, M.; Gumbsch, P. Structural Relaxation Made Simple. *Phys. Rev. Lett.* **2006**, *97*, 170201.
(52) Guénolé, J.; Nöhring, W. G.; Vaid, A.; Houllé, F.; Xie, Z.; Prakash, A.; Bitzek, E. Assessment and Optimization of the Fast Inertial Relaxation Engine (FIRE) for Energy Minimization in Atomistic Simulations and Its Implementation in LAMMPS. *Comput. Mater. Sci.* **2020**, *175*, 109584.
(53) Yang, H.; Huang, S.; Huang, X.; Fan, F.; Liang, W.; Liu, X. H.; Chen, L.-Q.; Huang, J. Y.; Li, J.; Zhu, T.; Zhang, S. Orientation-Dependent Interfacial Mobility Governs the Anisotropic Swelling in Lithiated Silicon Nanowires. *Nano Lett.* **2012**, *12*, 1953−1958.
(54) Schmidt, H.; Jerliu, B.; Hüger, E.; Stahn, J. Volume Expansion of Amorphous Silicon Electrodes during Potentiostatic Lithiation of Li-Ion Batteries. *Electrochem. Commun.* **2020**, *115*, 106738.
(55) Mendez, J. P.; Ponga, M.; Ortiz, M. Diffusive Molecular Dynamics Simulations of Lithiation of Silicon Nanopillars. *J. Mech. Phys. Solids* **2018**, *115*, 123−141.
(56) Wang, B.; Réthoré, J.; Aifantis, K. E. Capturing the Stress Evolution in Electrode Materials That Undergo Phase Transformations during Electrochemical Cycling. *Int. J. Solids Struct.* **2021**, *224*, 111032.
(57) Yao, Y.; McDowell, M. T.; Ryu, I.; Wu, H.; Liu, N.; Hu, L.; Nix, W. D.; Cui, Y. Interconnected Silicon Hollow Nanospheres for Lithium-Ion Battery Anodes with Long Cycle Life. *Nano Lett.* **2011**, *11*, 2949−2954.
(58) McDowell, M. T.; Lee, S. W.; Harris, J. T.; Korgel, B. A.; Wang, C.; Nix, W. D.; Cui, Y. In Situ TEM of Two-Phase Lithiation of Amorphous Silicon Nanospheres. *Nano Lett.* **2013**, *13*, 758−764.
(59) Liu, X. H.; Zhong, L.; Huang, S.; Mao, S. X.; Zhu, T.; Huang, J. Y. Size-Dependent Fracture of Silicon Nanoparticles during Lithiation. *ACS Nano* **2012**, *6*, 1522−1531.

https://doi.org/10.1021/acsami.1c02977
ACS Appl. Mater. Interfaces 2021, 13, 21310−21319